STRONG AND TOUGH STEEL WELDS

Murugananth M.[1], Bhadeshia H. K. D. H.[1], Keehan E.[2], Andrén H. O.[2], Karlsson L.[3]
[1]Department of Material Science and Metallurgy, University of Cambridge, U.K
[2]Department of Experimental Physics, Chalmers University of Technology, Gothenburg, Sweden
[3]ESAB AB, Gothenburg, Sweden

ABSTRACT

It is frequently observed that the toughness of a steel or steel weld metal decreases as it is strengthened. Brittle failure occurs when the stress required to cleave the metal becomes small compared with that needed to cause gross plastic deformation. It is natural therefore, that anything which makes plastic flow more difficult must lead to a greater risk of brittle failure unless something is done also to improve the resistance to cleavage.

It is common to add nickel to a ferritic steel in order to enhance toughness. However, our calculations using neural network models showed that nickel does not in fact improve the toughness at high concentrations of manganese. It is predicted that nickel only enhances toughness when the manganese concentration is low.

These calculations have been verified experimentally and it is demonstrated that the *predicted* large improvement in toughness can indeed be achieved in practice. A considerable amount of work has been done to investigate the mechanism of the nickel-manganese effects. X-ray diffraction was used to measure the amount of retained austenite. Microstructural studies done using optical and scanning electron microscopy showed mixed microstructures of bainite and martensite.

Dilatometric analysis revealed that as expected, the low manganese alloys had a higher Ac_1 temperature. This, in combination with tempering effects seem to lead to a combination of soft and hard metal in the material exposed to a Charpy test. Possible mechanisms are proposed for the Ni–Mn effect in relation to the improved toughness of high nickel low manganese welds.

INTRODUCTION

Ferrite has the major disadvantage that it undergoes a ductile–brittle transition at low temperatures or high strain rates. The fracture mode changes from one involving significant plastic deformation to cleavage (fig. 1). This is because the flow stress of ferrite is very sensitive to temperature and eventually becomes larger than necessary to cleave the crystals.

Mathematical Modelling of Weld Phenomena - VI
Published by the Institute of Materials, eds H. Cerjak and H. K. D. H. Bhadeshia, 2002, 205-230.
M. Murugananth, H. K. D. H. Bhadeshia, E. Keehan, H. O. Andren and L. Karlsson

In the context of weld metals, work by Lord [1] focused on improving the toughness of a nickel-containing commercial ferritic-weld electrode OK 75.78 (Charpy value at -60 °C : 55 J, table 1), used for applications where toughness is critical. Many alloy variants were produced but none managed to match the combination of strength and toughness of OK 75.78 (fig. 2). Nickel additions in this case did not lead to improved toughness.

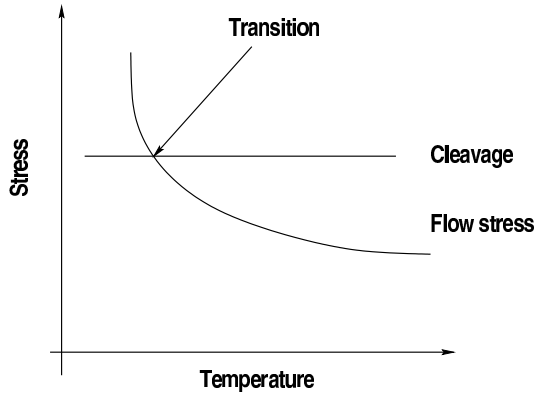

Figure 1: Schematic diagram of illustrating the ductile-brittle transition in ferrite.

C	Mn	Si	P	S	Cr	Ni	Mo
0.05	2	0.3	0.005	0.012	0.5	3	0.6

Table 1: Typical all-weld metal composition of commercial welding electrode OK 75.78 in wt%

The purpose of the work presented here was to adopt a different approach, involving a combination of mathematical models which were used to explore ways of improving both the toughness and strength, using nickel as the primary alloying addition to ferritic weld metals.

EXPERIMENTAL DETAILS

Manufacture of weld metals

All the welds were fabricated using the manual metal arc (MMA) process from experimental electrodes produced to our composition specification at the ESAB AB Central Laboratories, Gothenburg, Sweden. As this work focuses upon the weld

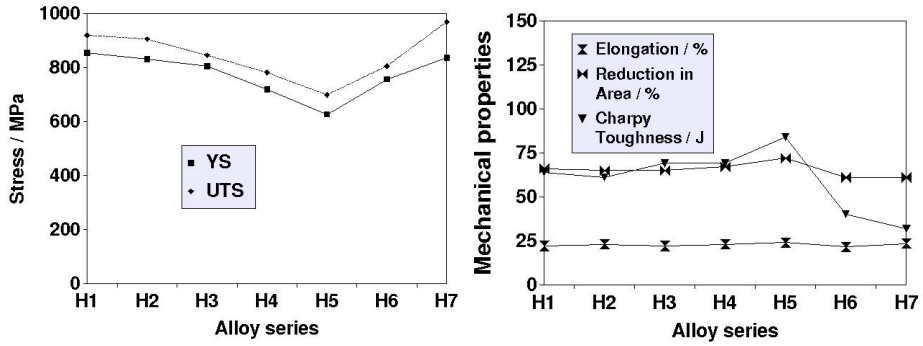

Figure 2: Mechanical properties of a series of experimental welds (H1-H7) due to Lord [1]. Weld H1 is the commercial electrode OK 75.78. The Charpy toughness is for -60 °C. The compositions of welds H1-H7 are listed in table 2.

metal itself, a particular joint geometry (ISO 2560) was chosen to reduce the effects of dilution due to mixing with the base metal. The welds were fabricated using 20 mm thick plates. Three experimental welds designated A, B and C (described later) were fabricated. Weld A and B consisted of 22 beads using a heat input of 1.1 kJ mm^{-1}, whereas weld C contained 24 beads with a heat input of 1.0 kJ mm^{-1}. An interpass temperature of 250 °C was specified. Buttering of the plates was performed prior to welding, involving the deposition of a layer weld beads along the edge of the plates.

Dilatometry using Thermecmastor Z thermomechanical simulator

The *Thermecmastor Z* allows the computer controlled application of heat treatments and deformation to a sample of material. Laser dilatometry is used to follow phase transformations as they occur, where the temperature is recorded using a Pt-PtRh thermocouple attached to the sample. The experiments are performed in a sealed chamber which is usually evacuated to allow efficient cooling of the specimen and to prevent oxidation. The specimen is seated centrally between Si_3N_4 platens. Heating is via a water-cooled induction coil surrounding the specimen. The maximum heating rate that can be achieved is around 50 °C s^{-1} but this is dependent upon the material. Cooling is controlled using helium jets. The specimens are usually solid cylinders of length 12 mm and diameter 8 mm. For experiments in which rapid cooling is required, better results are achieved using hollowed out specimens with an internal diameter of 5 mm. A scanning laser beam is used to measure the di-

Element /wt%	Weld						
	H1	H2	H3	H4	H5	H6	H7
Carbon	0.049	0.037	0.045	0.026	0.025	0.022	0.102
Manganese	2.09	2.13	1.11	0.97	0.85	0.78	2.18
Silicon	0.29	0.27	0.29	0.23	0.022	0.17	1.63
Phosphorus	0.005	0.010	0.008	0.010	0.010	0.010	0.009
Sulphur	0.012	0.006	0.006	0.010	0.009	0.011	0.005
Chromium	0.43	0.46	0.43	0.44	0.03	0.03	0.02
Nickel	3.04	3.03	3.91	4.00	3.91	4.25	2.07
Molybdenum	0.59	0.60	0.58	0.61	0.60	0.13	0.23
Vanadium	0.019	0.019	0.016	0.015	0.015	0.011	0.019
Copper	0.03	0.03	0.03	0.03	0.03	2.18	0.03
Titanium	0.014	0.014	0.014	0.012	0.012	0.010	0.039
Tin	0.007	0.010	0.007	0.004	0.002	0.001	0.010
Arsenic	0.012	0.012	0.012	0.006	0.005	0.000	0.013
Boron	0.0005	0.0006	0.0004	0.0002	0.0001	0.0000	0.0007
Oxygen	0.0267	0.0307	0.0310	0.0348	0.0299	0.0423	0.0205
Nitrogen	0.0118	0.0143	0.0101	0.0143	0.0148	0.0125	0.0113
Iron	bal.	bal.	bal.	bal.	bal.	bal.	bal.

Table 2: Compositions of series of welds studied by Lord [1]

ameter of the specimen during testing. A thermocouple is attached to the specimen using spot welding and, on placing the specimen in the machine, the thermocouple is located in order to prevent interference with the dilatometry measurements. Data from the dilatometer, the thermocouple and the load cell are logged simultaneously by a computer for later analysis.

Temperature dependence of hardness

In order to measure the hardness as a function of temperature below ambient, the weld metal sample was placed in a metallic container filled with liquid nitrogen (fig. 3). The liquid nitrogen was allowed to evaporate and as the sample warmed up, hardness measurements were performed.

X-ray diffraction

The retained austenite content was measured using X-ray diffraction (Cu-K_α with wavelength, λ : 1.5418 Å). Metallographically polished samples were chemically etched to remove the deformed layer, and then step–scanned over the 2θ range 47-130°. After indexing, the retained austenite content was determined by choosing three peaks (to account for texture effects [2]) of austenite corresponding to the planes (002), (022) and (113). The amount of specimen area illuminated by the

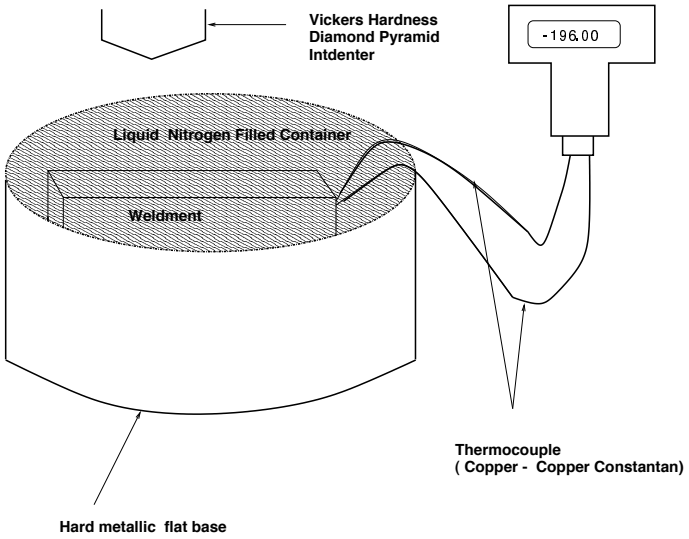

Figure 3: Experimental equipment for the measurement of hardness as a function of temperature.

X-ray beam depends on the divergence slit used. In the present case, a divergence slit of $\frac{1}{2}^{\circ}$ was used, giving an illumination of $(15\pm3)\times(3\pm1)$ mm^2 on the welds.The measurements were conducted in each case such that the weld centerline, along the cross-section, was illuminated, but it is not possible to comment on its exact location. The method used is better described in [3]. The computer program used for the calculation purposes can be found in [4].

Mechanical testing

All mechanical testing was done on samples machined from the weld metal itself. Cylindrical tensile specimens, 10 mm in diameter were machined along the weld direction. The specimens were degassed at 250 °C for 16 h prior to testing.

Standard 10 mm $\times$ 10 mm Charpy V-notch specimens were machined such that the position of the notch lay within the weld metal and the axis of the specimen was normal to the welding direction. Both the Charpy and tensile specimens were machined from the center of the welds.

Metallography

For optical metallography, the samples were etched using 2% nital. Scanning electron microscopy was also conducted on etched specimens using a Phillips XYZ20 microscope in the secondary electron mode.

INITIAL APPROACH

It is frequently stated that nickel improves the toughness of ferrite. At sufficiently large concentrations, nickel can also induce the formation and retention of austenite in the final microstructure. Yano *et al.* [5] developed a heat treatment process in which the steel is partially austenitised in the ferrite-austenite phase field and then quenched. This was found to give an improvement in toughness due to the presence of finely dispersed austenite islands stable at -196 °C, which hinder cleavage crack propagation. Austenite probably improves the toughness as follows [6] :

1. A propagating crack loses the stress concentration at its tip when in contact with ductile austenite which deforms and blunts the crack.
2. Detrimental impurity elements like phosphorus and sulphur are rendered harmless by solution in austenite.
3. Stress–induced transformation of austenite into martensite can relieve the stresses at the crack tip.

Based on these potentially desirable features of austenite, an empirical attempt was made to improve toughness by increasing the nickel concentration of H1 from 3 wt% to 7 wt% (weld A) and 9 wt% (weld B).
Nickel additions have the following known consequences :

1. They decrease the Ac_1 temperature which makes it easier to obtain austenite during the tempering encountered in multipass welds.
2. They stabilise austenite at subzero temperatures.
3. They lead to the introduction of retained austenite between low carbon martensite laths in the microstructure. Calculations using the Koistnen and Marburger equation [7] indicated about 2.6 % by volume of retained austenite in the microstructure of weld A. Experimental measurements using X-ray diffraction analysis are discussed under separate headings.
4. Engel-Brewer correlations indicate that the cohesive energy is determined by the number of s, p and d bonding electrons [8]. If an assumption is made that toughness increases with cohesive energy, then there is a basis for predicting the effect of elements in solid solution on the toughness of ferrite, since the cohesive energy increases smoothly with the number of s, p, d electrons. Thus, nickel, palladium and platinum have a large excess of electrons in comparision

Element	Weld A	Weld B	Weld C
All elements in wt% unless otherwise specified			
C	0.03	0.03	0.025
Si	0.25	0.25	0.37
Mn	2	2	0.65
S	0.01	0.01	0.006
P	0.01	0.01	0.013
Ni	7.3	9.2	6.6
Cr	0.5	0.5	0.21
Mo	0.62	0.62	0.4
V	0.011	0.011	0.011
Cu	0.04	0.04	0.03
Co	0.009	0.009	0.009
W	0.005	0.005	0.005
O / ppm	330	320	380
Ti / ppm	80	80	80
N / ppm	120	140	180
B / ppm	10	10	1
Nb / ppm	10	10	10

Table 3: Manufactured compositions of welds A, B and C. Weld C is discussed later in the paper.

with α Fe and should therefore increase toughness by making cleavage more difficult.

Time-Temperature-Transformation diagrams (fig. 4) calculated as in [9] provide evidence of an increase in hardenability even with 7 wt % nickel in weld A, indicating that in a homogeneous sample, low-carbon martensite should be obtained at all reasonable cooling rates. All these considerations indicated that the toughness should improve with the addition of nickel, but in practice, the welds with 7 wt% and 9 wt% were brittle with only 15 J and 14 J respectively recorded in Charpy tests conducted at -60 °C. Yield strengths were comparable to that of H1 for both welds A and B with 789 MPa and 841 MPa respectively. Following this failure in intuitive design, a more quantitative approach was adopted.

TOUGHNESS-STRENGTH RELATIONSHIPS

Artificial neural network (ANN) models for the yield and ultimate tensile strength, toughness and elongation, were created from an experimental database representing 3300 ferritic welds, which included the experimental results from the 7 wt% and

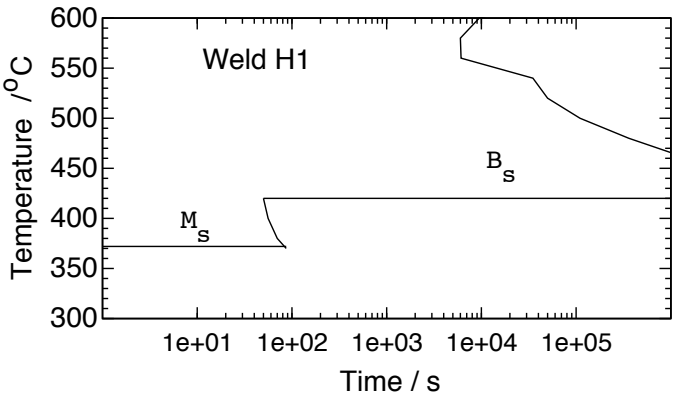

(a)

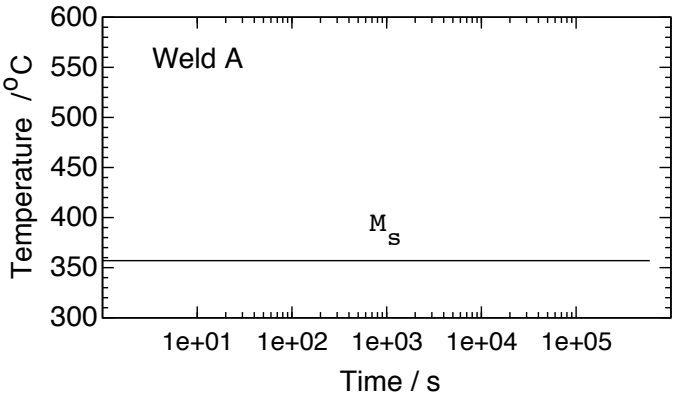

(b)

Figure 4: Time-temperature-transformation (TTT) diagrams showing the M_s and the B_s(bainite–start temperature). The curves represent onset of transformation.(a) H1–3 wt% Ni. (b) Weld A - higher hardenability as no reconstructive transformation is observed even after 10^5 s

9 wt% nickel welds. The description of the method itself can be found elsewhere [10, ?, 11]. The database consisted of information from multi-run weld deposits designed for low-dilution to enable specifically the measurement of all-weld metal properties. They (data) all represent electric arc welds made using one of the following processes: manual metal arc (MMA), submerged arc welding (SAW) and tungsten inert gas (TIG). The spread of the data is as shown in figures 5, 6, which show that carbon, manganese, nickel, oxygen, interpass temperature and heat input are uniformly represented, although this assessment could be flawed since each graph only represents one variable. However, the Bayesian inference in the neural network method used is able to indicate regions of the input space where data are sparse by implementing a larger uncertainity (error bar) in that region.

The base set of input variables (table 4) used in training of the models comprised of chemical composition, welding parameters, heat treatment and the temperature at which the Charpy toughness tests were conducted.

Oxygen was an input variable for the toughness, ultimate tensile strength and elongation models since the inclusion content has an effect on all these properties, but not on yield strength where oxygen was excluded.

Fig. 7 illustrates the overall behaviour of each of the committee of models (for definition of committees see [10]). The error bars illustrated represent the uncertainities in the predictions; a further contribution to the error comes from noise, which is not illustrated. The maximum perceived noise in the output for toughness, yield strength, ultimate tensile strength and elongation was 0.0833, 0.04024, 0.0232 and 0.0638 respectively, when each output scales from 0 to 1. The models used are freely available on [12].

NEURAL NETWORK PREDICTIONS

The toughness was then estimated as a function of nickel and manganese concentrations with the other variables controlled as in table 5.

The results (fig. 8) revealed a remarkable trend, that for the system studied, nickel only leads to an improvement in toughness when the manganese concentration is small. It is otherwise detrimental to toughness. This prediction is consistent with experimental data reported recently by Kang *et al.*[13].

Following this analysis, a new experimental weld was manufactured with a manganese concentration below 0.7 wt% (weld C in table 6).

The actual composition of weld C (as opposed to its design composition) was analysed using the ANN model and the results are illustrated in fig. 9. They show

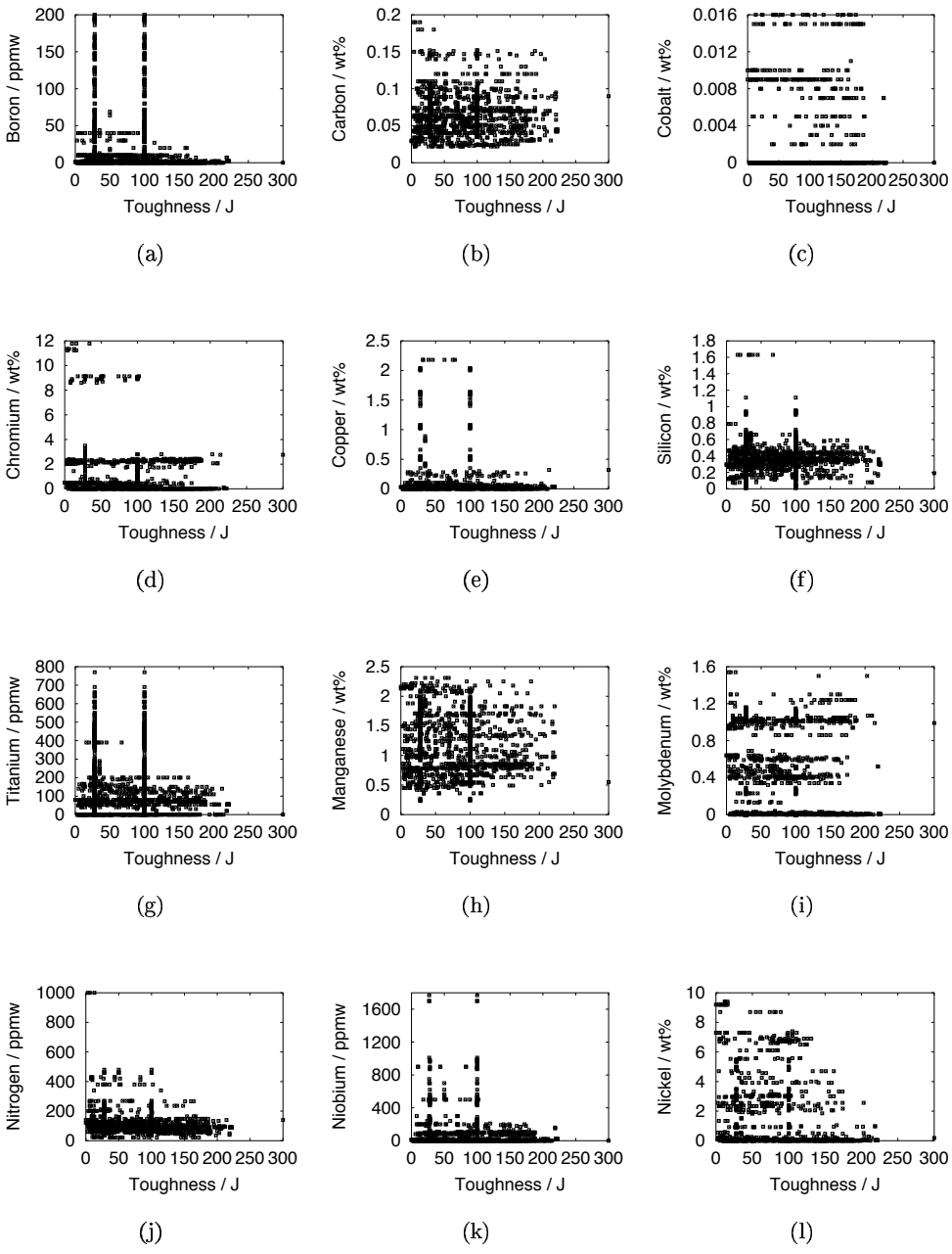

Figure 5: The one-dimensional distribution of data

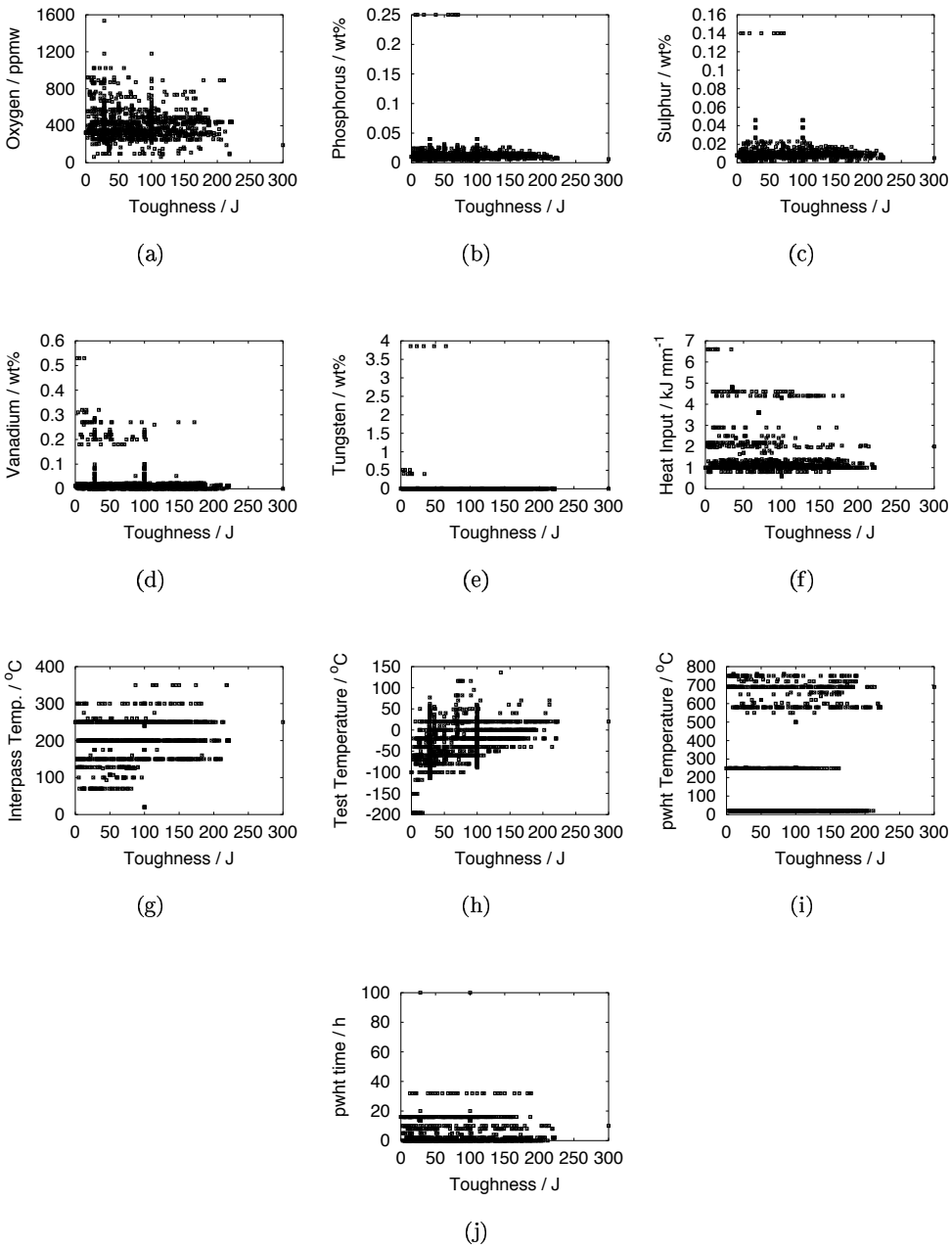

Figure 6: The one-dimensional distribution of data

	Input variables	Minimum	Maximum	Mean	Standard Deviation
All elements in wt% unless otherwise specified					
1	Carbon	0.02	0.19	0.07	0.021
2	Silicon	0.01	1.63	0.4	0.13
3	Manganese	0.23	2.31	1.2	0.42
4	Sulphur	0.002	0.14	0.0078	0.008
5	Phosphorus	0.003	0.25	0.01	0.014
6	Nickel	0	9.4	0.6	1.6
7	Chromium	0	11.78	0.5	1.4
8	Molybdenum	0	1.54	0.2	0.34
9	Vanadium	0	0.53	0.01	0.045
10	Copper	0	2.18	0.06	0.22
11	Cobalt	0	0.016	0.0007	0.0027
12	Tungsten	0	3.8	0.008	0.2
13	Oxygen / ppm	63	1535	406.2	112.3
14	Titanium / ppm	0	770	100.03	135.4
15	Nitrogen / ppm	21	1000	98.3	67.8
16	Boron / ppm	0	200	13.8	34.3
17	Niobium / ppm	0	1770	39.3	136.8
18	HI[a] / kJ mm^{-1}	0.6	6.6	1.19	0.7
19	IT[b] / °C	20	350	200.19	31.23
20	pwhtT [c] / °C	20	760	185.36	257.24
21	pwhtt[d] / h	0	100	2.7	6.13
22	Test temperature / °C	-196	136	-44.25	36.13

Table 4: Input variables used to train the models for establishing a network of composition, heat treatment and welding parameters with toughness, yield strength, toughness and ultimate tensile strength.

[a]Heat input
[b]Interpass temperature
[c]post-weld heat treatment temperature
[d]post-weld heat treatment time

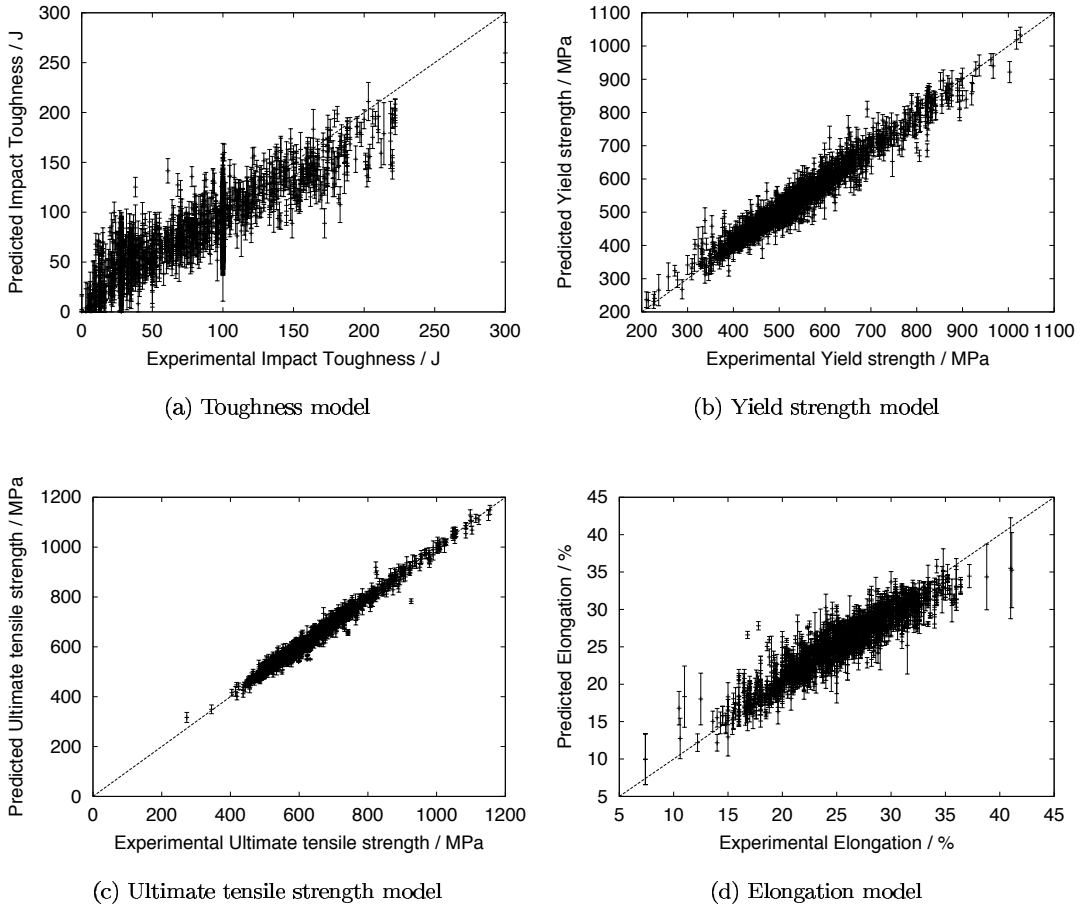

(a) Toughness model

(b) Yield strength model

(c) Ultimate tensile strength model

(d) Elongation model

Figure 7: A comparison of calculations against measured data for a variety of mechanical properties, covering some 3300 experiments.

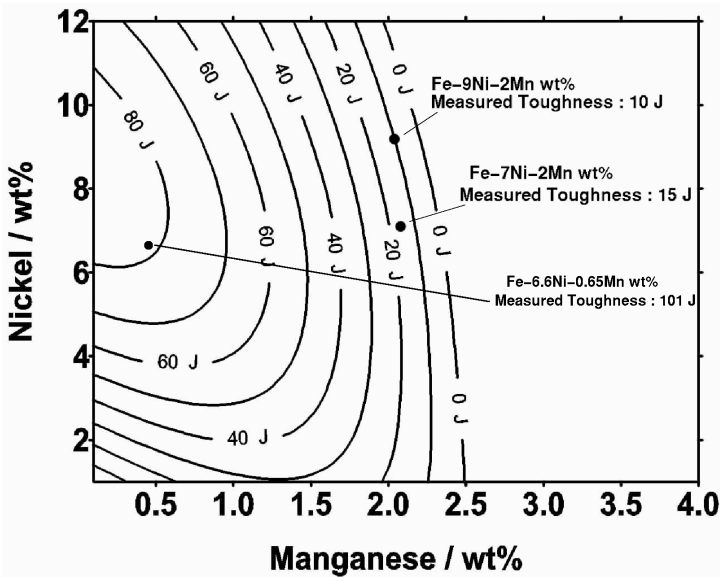

(a)

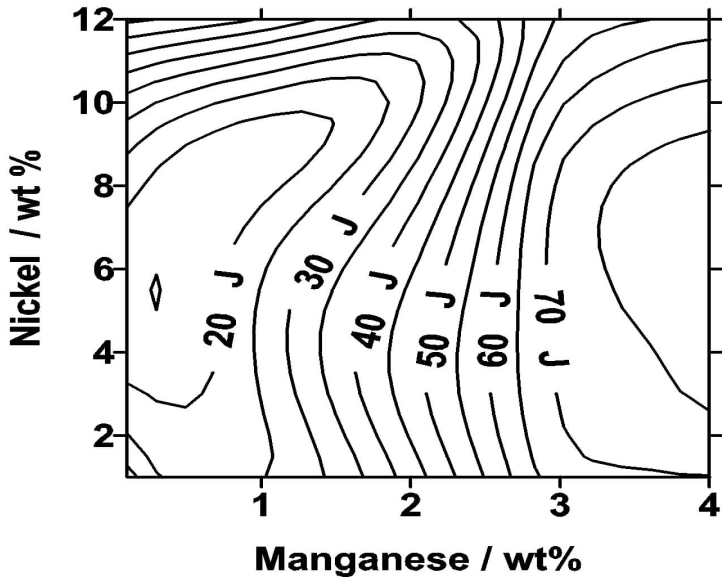

(b)

Figure 8: Effect of manganese and nickel concentrations on toughness at -60°C, as predicted using the neural network models. (a) Predictions. (b) Uncertainity in prediction.

C	Si	Mn	S	P	Ni	Cr	Mo
0.034	0.25	0-2	0.008	0.01	0-12	0.5	0.62
V	Cu	Co	W	O / ppm	Ti / ppm	N / ppm	B / ppm
0.011	0.04	0.009	0.005	380	80	250	1
Nb / ppm	HI / kJ mm^{-1}	IT / °C	pwhtT / °C	pwhtt / h			
10	1	250	250	16			

Table 5: Base composition used for analysing the effects of nickel and manganese concentrations. All elements are in wt% unless otherwise specified.

C	Si	Mn	S	P	Ni	Cr	Mo
0.025	0.37	0.65	0.006	0.013	6.6	0.21	0.4
V	Cu	Co	W	O / ppm	Ti / ppm	N / ppm	B / ppm
0.011	0.03	0.009	0.005	380	80	180	1
Nb / ppm	HI / kJ mm^{-1}	IT / °C	pwhtT / °C	pwhtt / h			
10	1	250	250	16			

Table 6: Manufactured composition of experimental weld C measured using optical emission spectrometry and Leco combustion equipment.

that increasing the nickel beyond 8 wt% should not be beneficial for toughness. Chromium and molybdenum have little effect on toughness. The essential outcome of the analysis is that the composition of weld C, as given in table 6, is in fact optimum in the sense that positive or negative deviations from the values of nickel and managanese concentrations given in table 6 reduce toughness. Of course this does not mean that some other combination of alloying elements may not lead to better results. Even the trace elements are well-controlled.

Heat input and interpass temperature do have significant effects because they determine the weld cooling rate. A higher cooling rate, lower heat input or lower interpass temperature reduce the toughness because they lead to an increase in strength (figs 11a, 11b).

MECHANICAL PROPERTIES AND MICROSTRUCTURE

Weld C was found to be much tougher than welds A and B, at all testing temperatures (fig. 12). Its yield strength however was slightly lower (table 7). Comparison of welds A and C, having similar nickel concentrations, shows that there is a large increase in toughness from 15 J (weld A & B) to 101 J at -60 °C, although with a small reduction in yield strength from 789 MPa (weld A) to 725 MPa (weld C). The

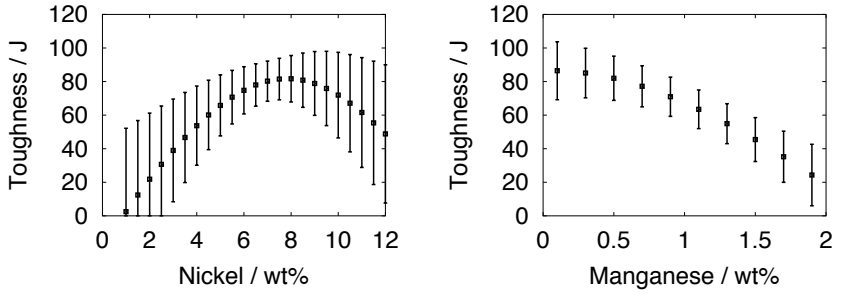

(a)

(b)

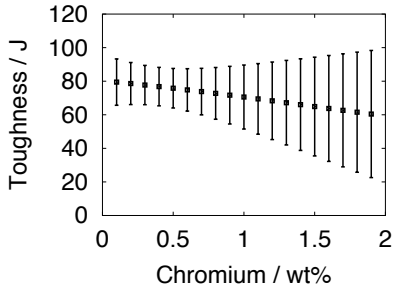

(c)

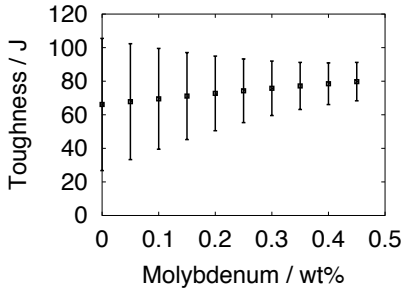

(d)

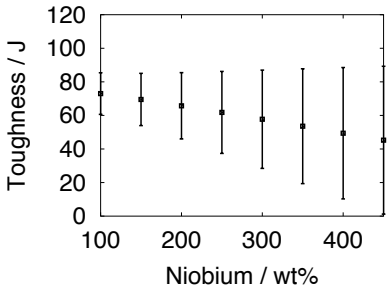

(e)

Figure 9: Effect of variation in concentration of alloying elements on toughness of weld C at a test temperature of - 60 °C.

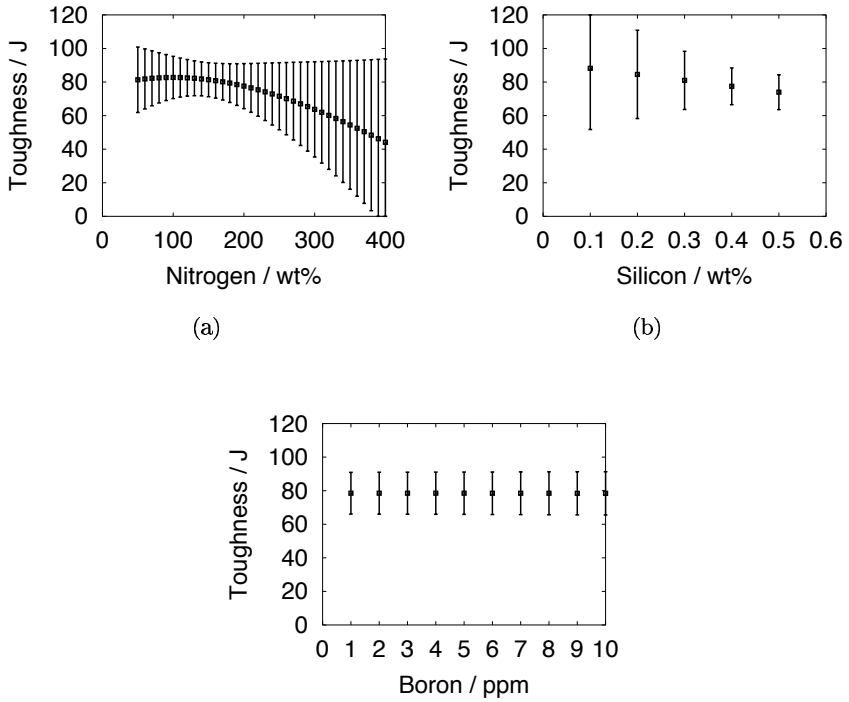

Figure 10: Effect of variation in concentration of alloying elements on toughness of weld C at a test temperature of - 60 °C.

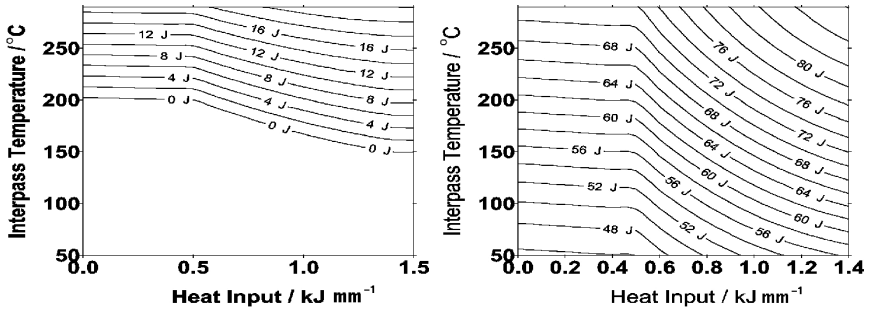

(a) Weld A (b) Weld C

Figure 11: Effect of variation of heat input and interpass temperature on toughness of welds A and C at a test temperature of -60 °C.

	Weld A	Weld B	Weld C
Yield strength (YS) / MPa	789	841	725
Ultimate tensile strength (UTS) / MPa	1009	1055	822
Elongation / %	14.8	14	21.4
YS/UTS	0.78	0.80	0.87

Table 7: Mechanical properties of welds A, B and C

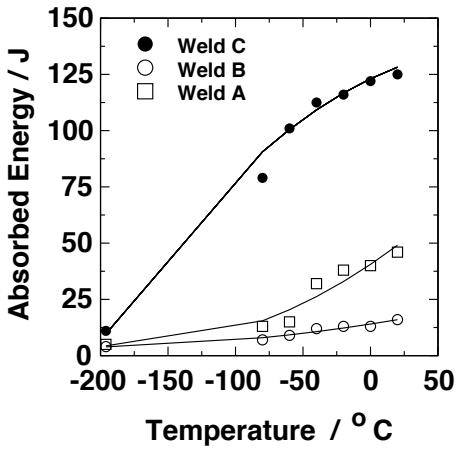

Figure 12: Effect of temperature on the absorbed energy of welds A, B and C during Charpy impact test.

decrease in yield strength does not seem large enough to explain the huge increase in toughness obtained by lowering the manganese concentration, but the result is a striking confirmation of the neural network calculations illustrated in fig. 8.

Comparison of toughness should strictly be conducted at constant strength. A study of the temperature dependence of the flow stress for welds A and C was done by measuring the hardness as a function of temperature in the hope that the toughness of the two welds could be compared at constant hardness. However, as shows in fig. 13, the hardness curves are almost horizontal as a function of temperature and sufficiently apart to prevent such a comparison.

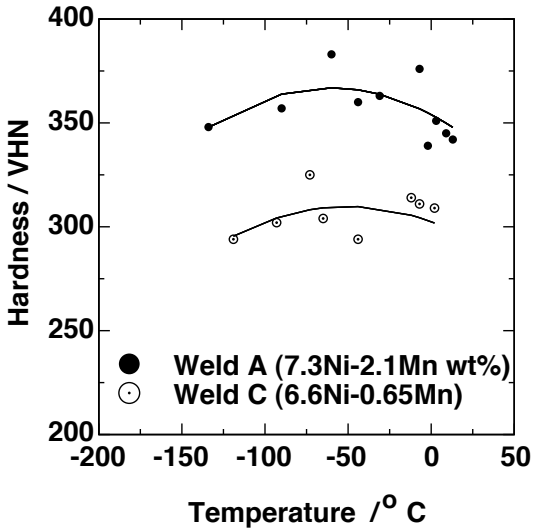

Figure 13: Temperature dependence of the hardness of the top bead from welds A and C.

However, a limited account can be taken of the influence of strength by comparing the Charpy toughness at -60 °C against the yield strength of welds H1–H7, A, B and C. Fig. 14 shows that welds A and B, in spite of the high nickel concentrations, have very poor toughness when compared with welds H1 and H3 respectively which match in terms of strength. On the other hand, weld C shows an improvement in toughness when compared against weld H4 which has identical strength. This strengthens the conclusion that weld C has improved toughness.

The results from X-ray diffraction experiments are illustrated in fig. 15. Retained austenite measurements are presented in table 8. The volume percentage of retained austenite is not particularly different for the three welds and hence is unlikely to explain any changes in toughness.

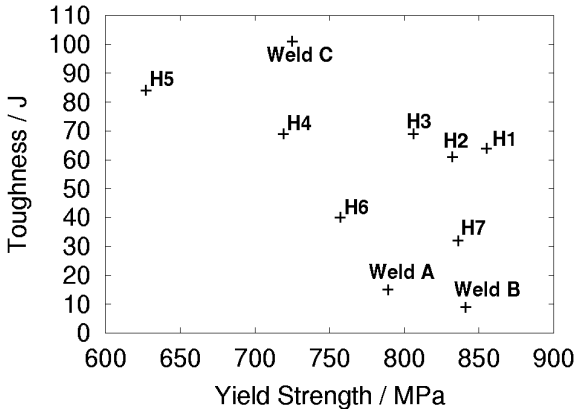

Figure 14: Charpy toughness measured at -60 °C against the yield strength.

Material	Retained austenite / volume %	Error/ %
Weld A	1.5	0.1
Weld B	0.8	0.1
Weld C	2.2	0.1

Table 8: Retained austenite content as measured using X-ray diffraction technique. More information can be found under Experimental Details.

Effect of alloying on Ac_1 and inhomogeneity in microstructure

The variation in hardness of a multipass weld is expected to depend on its Ac_1 temperature; this variation is on two scales, first because the deposition of a bead causes heat treatment of the underlying layer, and secondly a coarser scale effect because of tempering by the repeated deposition of layers. The scatter in strength/hardness of multipass welds is expected to depend on its Ac_1 temperature. This is because in a multipass weld, an increase in Ac_1 also increases the section of the material which is tempered. The severity of tempering also increases with Ac_1 [14].

With high Ac_1, in a multipass weld, a portion of the previous pass tempers whereas for lower Ac_1 alloys the previous pass largely reaustenises and transforms back to hard microstructures on cooling. Higher concentrations of austenite stabilising elements lead to a decrease in the Ac_1 temperature.

Dilatometric experiments were used to measure the Ac_1 temperature of each weld in which the sample was austenised at 1000 °C for 10 min at a heating rate

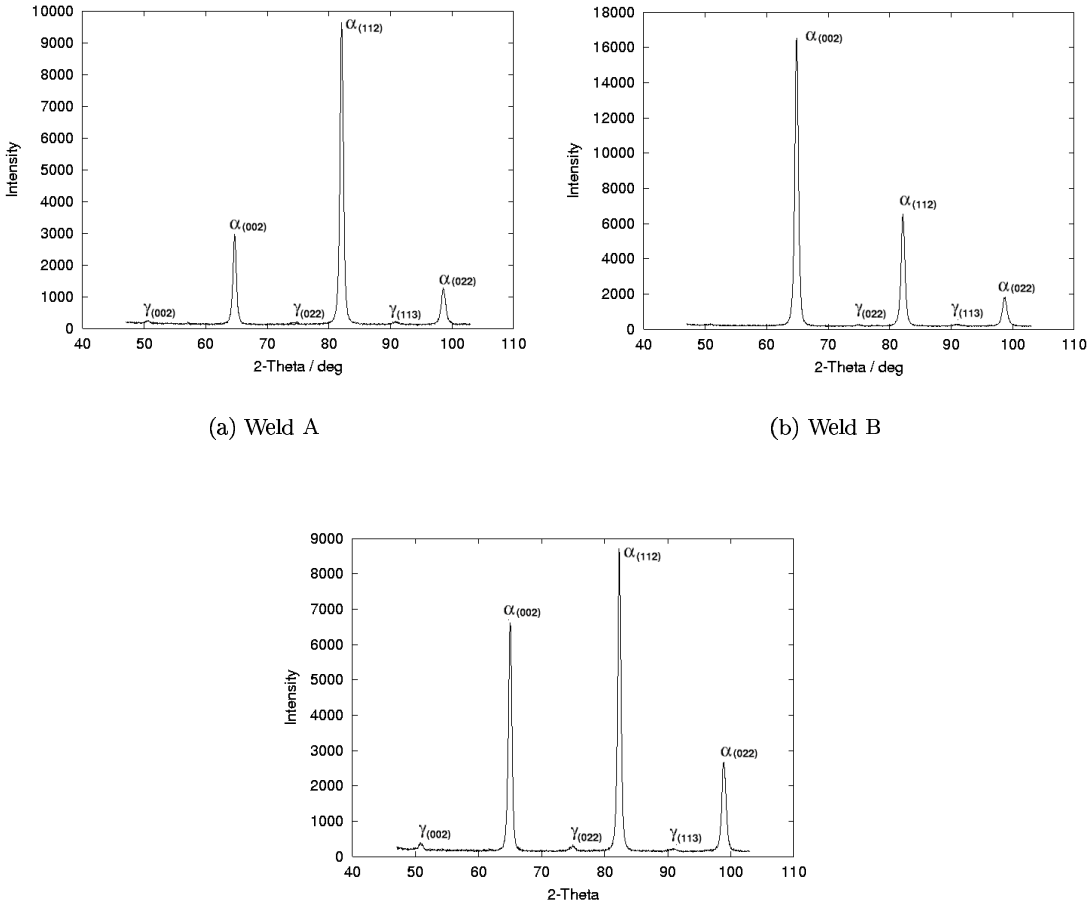

(a) Weld A

(b) Weld B

(c) Weld C

Figure 15: Intensity vs 2θ plots for Weld A, B and C showing the austenite and ferrite peaks.

of 10 °C s^{-1}. They were then cooled at a rate of 30 °C s^{-1} (typical weld cooling rate). This revealed that weld A with the higher alloy content has a lower Ac_1 temperature $\approx$ 650 °C (fig. 16a), whereas for weld C, $Ac_1 \approx$ 680 °C (fig. 16b). Although the difference in Ac_1 temperatures is only 30°C, it is consistent with the fact that the *variation* in hardness is greater in weld C, when measured on the weld centerline on a cross-section of the weld (fig. 17).

Fig. 16 also shows two effects which are reproducible but whose consequences are not yet understood. The temperature range over which austenite forms is greater for weld C. Also the total dilatation for weld A is almost twice that for weld C during austenite formation.

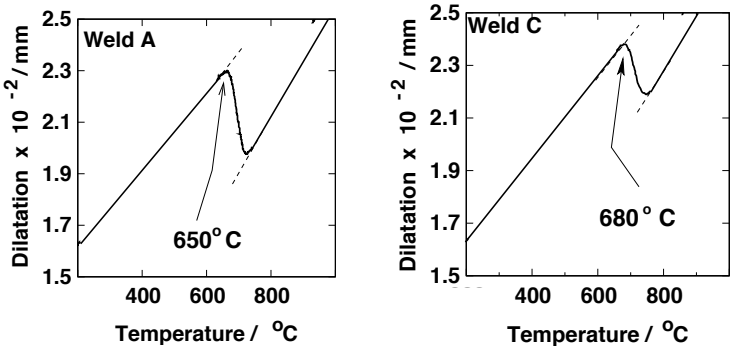

(a) Higher concentration of alloying elements

(b) Lower concentration of alloying elements

Figure 16: Dilatation curves for welds A and C, showing corresponding Ac_1 temperatures, obtained at a heating rate of 10 °C s^{-1} using a cylindrical sample of diameter 7 mm and height 12 mm.

Further experimental results

A variety of measurements were done on weld C, as a function of the interpass temperature. Fig. 18 shows a comparison of measured values against those predicted using neural network models; there is excellent agreement. It is emphasised that the experimental data were not used in creating the neural network model.

As–Deposited Microstructure

The microstructure of these welds is believed to consist essentially of a mixture of bainite and martensite [15]. It is useful to assess the as–deposited microstruc-

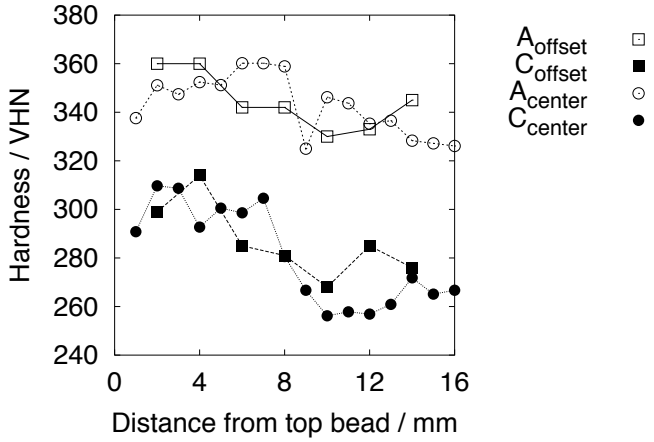

Figure 17: Variation in hardness along the depth, for welds A and C measured along the weld centerline and at a offset distance of 5 mm from the weld center.

ture using hardness tests. A sample from each weld was austenitised at 1000 °C and quenched in iced-brine in order to define the hardness of a fully martenisitic steel. The rule of mixtures can then be used (eq. 1) to find the relative amounts of martensite and bainite, from the hardnesses of the as–deposited microstructures (table 9).

$$H_m = V_{\alpha'} \times H_{\alpha'} + V_o \times H_o \tag{1}$$

where H_m is hardness of mixed microstructure (here martensite and bainite), $V_{\alpha'}$ is volume fraction of martensite, V_o is volume fraction of bainite, $H_{\alpha'}$ is hardness of martensite in water quenched sample, H_o is hardness of bainite in austenitised and very slowly cooled sample. It is evident that weld A has about 37 vol. % of bainite and weld C has about 92 vol. % of bainite, the remaining being martensite with some austenite.

	Hardness / VHN		
	Water quenched	Mixed Microstructure (As–deposited)	Annealed
Weld A	356	326	276
Weld C	315	279	276

Table 9: Vickers hardness of welds A and C. The hardness of the "mixed–microstructures" is that of the top, as–deposited weld metals, representing the average of 9 values in each case.

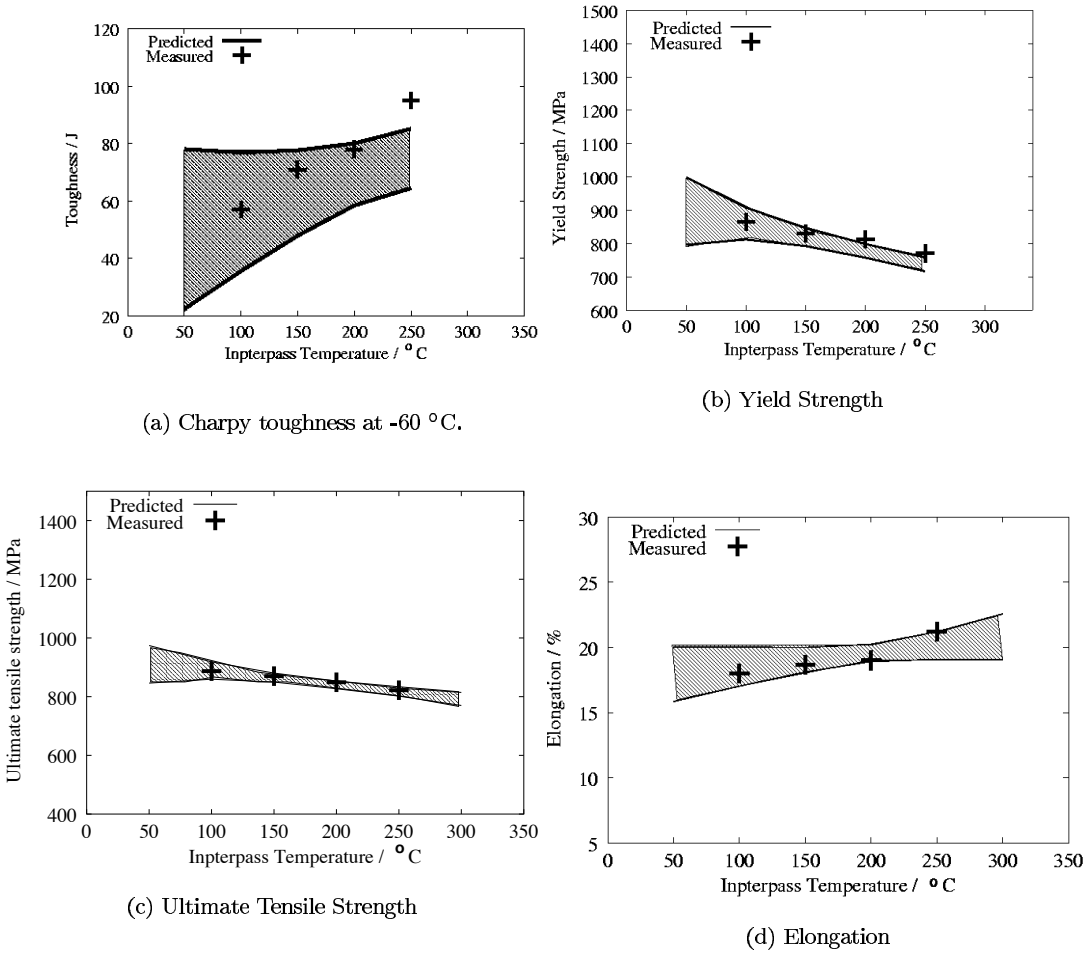

(a) Charpy toughness at -60 °C.

(b) Yield Strength

(c) Ultimate Tensile Strength

(d) Elongation

Figure 18: Comparison of measured and predicted mechanical properties, for composition of weld C with a heat input of 0.8 kJ mm^{-1}. The shaded bands represent the calculated values bounded by the estimated uncertainities in the calculations.

Alloying element	wt% in alloy	Partition Coefficient	wt% in solute–depleted regions
C	0.25	1	0.25
Si	0.37	0.71	0.26
Mn	0.65	0.76	0.49
Ni	6.6	0.46	2.9
Mo	0.4	0.49	0.19
Cr	0.21	0.83	0.18
V	0.011	0.76	0.009

Table 10: Thermodynamic calculations for element partitioning in weld C during solidification. The solute–depleted regions correspond to the cores of the solidifying entities [16].

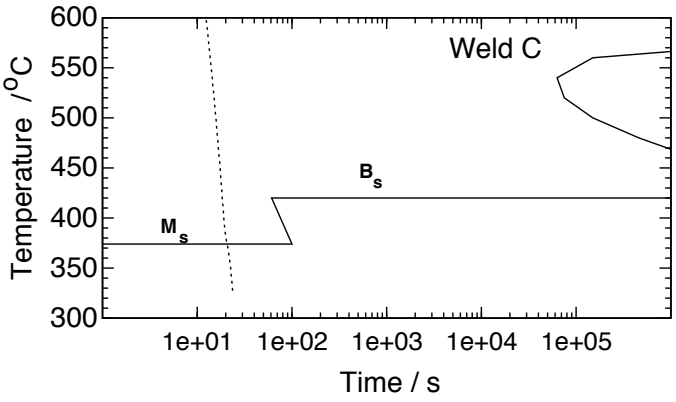

Figure 19: TTT diagram of weld C, along with a cooling curve depicting welding cooling rates.

However, the TTT diagram (fig. 19) for weld C indicates a fully martensitic structure, which of course is inconsistent with the hardness assessment described above. A look at low magnification optical micrograph revealed a lot of chemical segregation that occurred during solidification (fig. 20). Thermodynamic calculations were used to determine the solute partitioning during solidification under equilibrium conditions [16]. The partition coefficients along with the elements which segregate the most are listed in table 10. The TTT diagram for the solute–depleted region was then calculated [9]. This confirmed the possibility of bainite or Widmanstätten ferrite in the microstructure of segregated weld C (fig. 21), under theoretical equilibrium composition.

It would be tempting at this stage to conclude that the large difference in the mechanical properties of welds A and C is because the latter contains much more bainite. This remains to be established because the differences between marten-

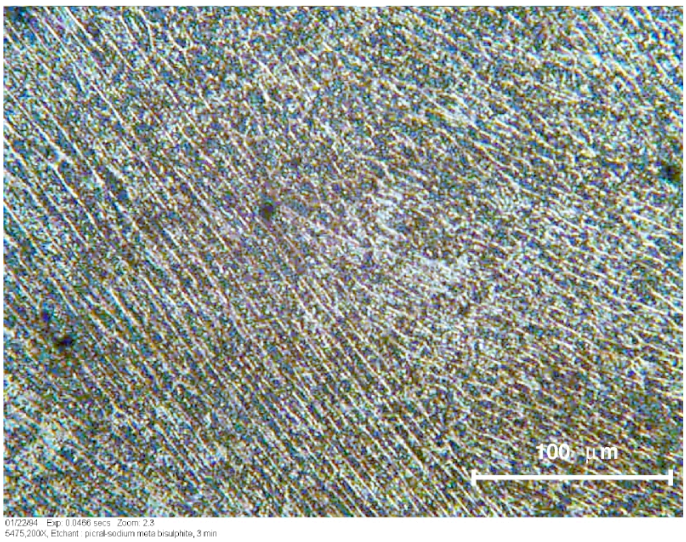

Figure 20: Cell structure observed in weld C roughly at the center of the weld, due to segregation during solidification.

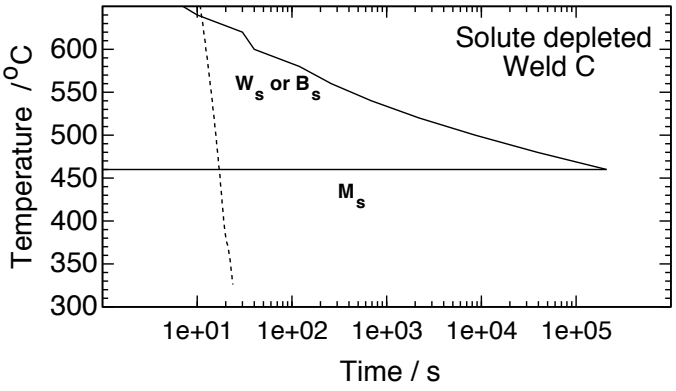

Figure 21: TTT diagram calculated for an alloy with the composition of the solute–depleted region described in table 10. A weld cooling curve is also plotted. The figure illustrates that it is possible to explain transformation in alloy C if there is sufficient solute segregation during solidification.

site and bainite become small as the carbon concentration is reduced to the levels in welds A–C. It is not therefore convincing to conclude that the *as-deposited* microstructure can explain the large differences in mechanical properties, although further detailed characterisation would be useful.

HARDNESS VARIATIONS

In the welds studied, nickel leads to an improvement in toughness if the manganese concentration is small. Charpy toughness measurements use samples which are 10 mm square cross-sections. An examination of fig. 17 shows that for welds A and B the hardness is uniformly high when measured on a cross-section, along the weld centerline over a distance of some 16 mm. Therefore, the Charpy test specimen, which has a V-notch, experiences this high hardness, which leads to poor toughness.

On the other hand, for weld C, the Charpy specimen experiences mainly the softened underlying weld metal.

It is possible to conclude therefore that the reduction in manganese at high nickel concentrations leads to a greater toughness because of the non-uniform hardness throughout the weld metal.

In future work, this will be verified by austenitising and quenching a sample of weld C to ensure a uniform hardness followed by Charpy tests to see whether the toughness deteriorates. It may be necessary to temper the quenched weld to ensure the same average yield strength to make a valid comparison. Microstructure will also be investigated in details.

SUMMARY

There is an undoubted demand for strong weld metals which have a high impact toughness at temperatures as low as -60 °C. It is frequently the case that nickel is added to strong steels in order to enhance toughness. However, all previous attempts on these lines have failed to produce the required combination of strength and toughness. This applies also to our intuitive approach where we simply increased the nickel concentration of an established commercial electrode.

An analysis of the problem using a set of neural network models of the mechanical properties of ferritic steel welds revealed that nickel is in fact detrimental to toughness when the manganese concentration is high. On the other hand, nickel greatly increases the energy absorbed in an impact test when it is added at low manganese concentrations. This revelation was tested successfully by manufacturing a low–Mn high–Ni manual metal arc welding electrode.

It remains to explain why there are contradictory effects of nickel as a function of the manganese concentration. Experiments demonstrated that the observations cannot be explained in terms of the amount of austenite retained in the microstructure.

A reduction in Ac_1 results in multipass welds which have a uniformly high hardness. By contrast, a high Ac_1 temperature results in greater tempering of the substrate layers, leading to a high hardness in the final layers but a softening of the initial layers.

However, the observed differences in Ac_1 are small so it is possible that the tempering resistance of high and low manganese alloys may differ and contribute to rapid softening; this could be a factor in addition to the Ac_1 effect and needs to be investigated further.But the fact that the low–Mn high–Ni allows shows substantial softening in the underlying passes must be significant. Bearing in mind that a Charpy sample has dimensions which span many layers of weld metal, it is expected that a lower toughness will be recorded when the hardness is uniformly high.

ACKNOWLEDGEMENTS

We are greatful to Prof. Fray for the provision of laboratory facilities, to the Cambridge Commonwealth Trust for financial support via a scholarship, to the council of Vice Chancellors and Principals for an ORS award, to ESAB AB for financial and material support and to Dr. D. J. C. MacKay for help with neural network analysis.

Bibliography

[1] M. Lord. *Design and Modelling of ultra-High Strength Steel Weld Deposits*. PhD thesis, University of Cambridge, March 1999.

[2] Dickson. *Acta Crystallographica*, 2:176–180, 1969.

[3] B. D. Cullity. *Elements of X-ray diffraction*. Reading, MA, Addison-Wesley, 1959.

[4] xrdcalc, http://www.msm.cam.ac.uk/map/map.html.

[5] S Yano. *Transactions ISIJ*, vol. 13:133–140, 1973.

[6] F. Darrel and J.W. Morris Jr. *Metallurgical Transactions A*, 17A:243–251, 1986.

[7] D. P. Koistinen and R. E. Marburger. *Acta Metallurgica*, 7:59–60, 1959.

[8] L. Brewer. *Alloying*. ASM International, Metals Park, Ohio, 1–28, 1988.

[9] H. K. D. H. Bhadeshia, L. E. Svensson, and B. Gretoft. *Acta Metallurgica*, 33:1271–1283, 1985.

[10] D. J. C. MacKay. *Neural Computation*, 4:448–472, 1992.

[11] H. K. D. H. Bhadeshia, D. J. C. MacKay, and L. E. Svensson. *Mater. Sci. Technol.*, volume 11:1046, 1995.

[12] David MacKay. In H Cerjak, editor, *Mathematical Modelling of Weld Phenomena, 3*, pages 359–389. Institute of Materials, 1997.

[13] http://www.msm.cam.ac.uk/map/map.html.

[14] B. J. Kang, H. J. Kim, and S. K. Hwang. *ISIJ International*, 40:1237–1245, 2000.

[15] R. C. Reed and H. K. D. H. Bhadeshia. In S. A. David and J. M. Vitek., editors, *Recent Trends in Welding Science and Technology*, pages 205–209, 1989.

[16] E. Keehan, L. Karlsson, M. Murugananth, H.O Andérn, and H. K. D. H. Bhadeshia. High strength steel weld metals–Developments with Ni and Mn. In *To be published in 7th Int. Welding Symposium of the Japanese welding society, kobe, Japan.*, Nov. 20–22 2001.

[17] D. Venugopalan and J. S. Kirkaldy. Hardenability concepts with applications to steels. In D. V. Doane and J. S. Kirkaldy., editors, *TMS-AIME*, pages 249–267, Warrendale, Pennsylvania, 1978.